MATERIALS SCIENCE

Negative-pressure polymorphs made by heterostructural alloying

Sebastian Siol,[1]*† Aaron Holder,[1,2] James Steffes,[3] Laura T. Schelhas,[4] Kevin H. Stone,[4] Lauren Garten,[1] John D. Perkins,[1] Philip A. Parilla,[1] Michael F. Toney,[4] Bryan D. Huey,[3] William Tumas,[1] Stephan Lany,[1] Andriy Zakutayev[1]*

Copyright © 2018 The Authors, some rights reserved; exclusive licensee American Association for the Advancement of Science. No claim to original U.S. Government Works. Distributed under a Creative Commons Attribution NonCommercial License 4.0 (CC BY-NC).

The ability of a material to adopt multiple structures, known as polymorphism, is a fascinating natural phenomenon. Various polymorphs with unusual properties are routinely synthesized by compression under positive pressure. However, changing a material's structure by applying tension under negative pressure is much more difficult. We show how negative-pressure polymorphs can be synthesized by mixing materials with different crystal structures—a general approach that should be applicable to many materials. Theoretical calculations suggest that it costs less energy to mix low-density structures than high-density structures, due to less competition for space between the atoms. Proof-of-concept experiments confirm that mixing two different high-density forms of MnSe and MnTe stabilizes a Mn(Se,Te) alloy with a low-density wurtzite structure. This Mn(Se,Te) negative-pressure polymorph has 2× to 4× lower electron effective mass compared to MnSe and MnTe parent compounds and has a piezoelectric response that none of the parent compounds have. This example shows how heterostructural alloying can lead to negative-pressure polymorphs with useful properties—materials that are otherwise nearly impossible to make.

INTRODUCTION

Polymorphism is the ability of a material to adopt multiple crystal structures, often with different properties. This natural phenomenon is so interesting that it has been featured in popular fiction, for example "ice-nine" from Kurt Vonnegut's *Cat's Cradle* (*1*). Polymorphism has also long fascinated researchers in various fields of science and technology. For example, mineral polymorphs can be used in geology to study temperature and pressure conditions long after a meteor impact (*2*), and the performance of drugs strongly depends on the conformation of the molecules in the pharmaceutical industry (*3*). The classical examples in solid-state chemistry include different properties in allotropes of carbon (inexpensive soft metal graphite versus expensive hard insulator diamond) (*4*) and varying photocatalytic activity in rutile versus anatase polymorphs of titanium dioxide (*5*).

Targeted synthesis of specific polymorphs remains a significant challenge in materials science (*6*). High-pressure synthesis is commonly used to stabilize high-density polymorphs with unique structure and properties, such as the optically transparent allotrope of sodium (*7*) or rocksalt (RS)–like polymorph of zinc oxide (*8*). In contrast, lower-density structures are much more difficult to access due to the inability to apply large enough tensile force ["negative pressure" (*9*)] to change the material structure. One technique that has been successfully used to achieve large negative pressure is thin-film epitaxy (*10*). However, this physical method can only apply tensile strain in two dimensions and, hence, is limited by a small critical film thickness of up to 10 to 100 nm (*11*). (Electro)chemical ion extraction or ion-exchange methods to achieve low-density materials are substrate-agnostic but are limited to small mobile atoms (for example, Li, Na, and Ne) and specific open structures (for example, Si, Ge, or H_2O ice clathrates) (*12*, *13*). Increasing the atomic volume of the material by isoelectronic alloying with larger ions [also known as "chemical pressure" in Fe-based superconductors (*14*)] and annealing the low-density precursors at high temperature [for example, in oxide perovskites (*15*)] can tune the material's properties, but without the ability to switch to a different lower-density crystal structure. It is likely that many new materials with useful properties would be discovered, if conditions equivalent to negative pressure could be realized.

In our recent publication (*16*), we have theoretically shown that mixing two compounds with different crystal structures ("heterostructural alloying") using nonequilibrium thin-film synthesis techniques can be used to access a broad range of chemical compositions, where no composition fluctuations or phase segregation occurs. This finding opened up new possibilities for designing materials functionality, as demonstrated for optoelectronic properties of $Mn_{1-x}Zn_xO$ alloys (*17*) and thermoelectric properties of $Sn_{1-x}Ca_xSe$ alloys (*18*). Here, we show that heterostructural alloying can be used to make materials that are stable only under large negative pressure and that such "negative-pressure polymorphs" can have unique properties that the parent compounds do not have. The present analysis goes well beyond the previous work, because it shows that, in addition to tuning structure and properties, heterostructural alloying can be used to synthesize new materials that are very dissimilar from the parent compounds and that are not possible to synthesize in any other way.

RESULTS

Thermodynamic and kinetic stability model

Consider a model compound A with three polymorphs α, β, and γ with different polymorph energies ΔE_A at different equilibrium atomic volumes V. As illustrated in Fig. 1A, at ambient pressure, the lowest enthalpy structure is α, and the two higher-enthalpy structures are β and γ. The α and β polymorphs are examples of high-density structures with smaller atomic volume, whereas γ represents a lower-density structure with larger atomic volume. Although high-pressure synthesis can be used to stabilize the high-density β polymorph of material A, access to its lower-density γ polymorph is limited by the inability to apply negative pressure.

[1]National Renewable Energy Laboratory, Golden, CO 80401, USA. [2]University of Colorado, Boulder, CO 80309, USA. [3]University of Connecticut, Storrs, CT 06269, USA. [4]SLAC National Accelerator Laboratory, Menlo Park, CA 94025, USA.
*Corresponding author. Email: andriy.zakutayev@nrel.gov (A.Z.); sebastian.siol@empa.ch (S.S.)
†Present address: Empa, Swiss Federal Laboratories for Materials Science and Technology, CH-8600 Dübendorf, Switzerland.

Downloaded from http://advances.sciencemag.org/ on May 11, 2018

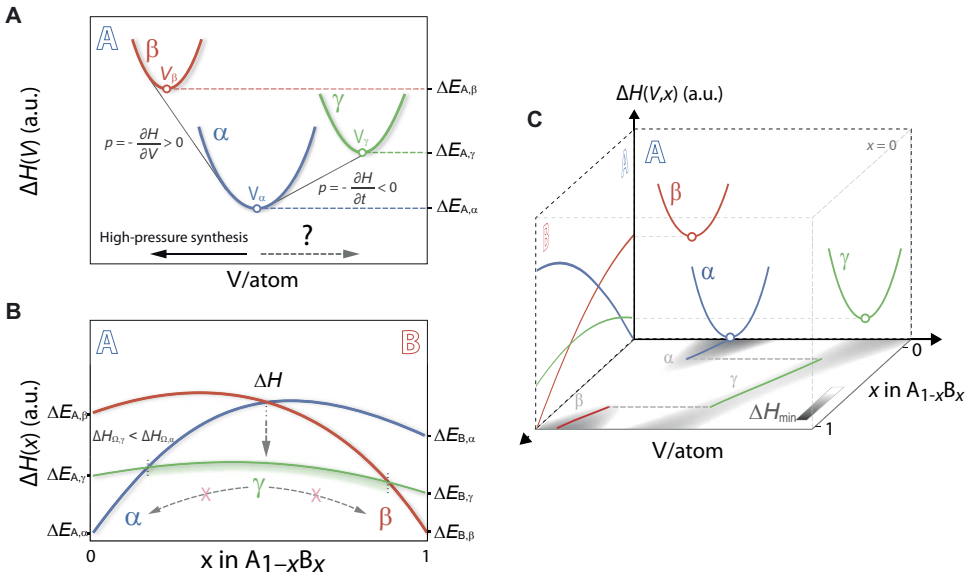

Fig. 1. Stabilization of negative-pressure polymorphs in heterostructural alloys. (**A**) Schematic illustration of α-, β-, and γ-polymorph enthalpies ΔH as a function of their respective atomic volume V and polymorph energies ΔE_A for a model compound A. Stabilization of lower-density polymorph γ would require negative pressure ($p = -\partial H/\partial V < 0$). (**B**) Polymorph enthalpies as a function of the alloying composition x in an alloy system $A_{1-x}B_x$ at equilibrium volume. Because of a smaller nonideal component of the mixing enthalpy $\Delta H_{\Omega,\gamma} < \Delta H_{\Omega,\alpha}$, the lower-density γ polymorph can become energetically favorable for intermediate alloying concentrations, if entropic stabilization or kinetic barriers prevent phase separation into α and β. (**C**) Grayscale projection of the minimum enthalpy $\Delta H_{min}(V,x)$ among the considered polymorphs outlines the basins of attraction for the three considered structures. The smaller bowing of the γ-polymorph enthalpy enables the stabilization of this high-volume structure by controlling the alloying concentration. a.u., arbitrary units.

However, in an alloy, the polymorph enthalpy ΔH depends not only on the formation enthalpy and the atomic volume but also on the enthalpic cost to mix the alloy constituents $\Delta H_{mix}(x)$. Thus, for a polymorph α in an alloy system $A_{1-x}B_x$, the enthalpy $\Delta H_\alpha(V,x)$ can be calculated as

$$\Delta H_\alpha(V,x) = \Delta H_{\mathrm{mix},\alpha}(x) + \Delta H_{\mathrm{vol},\alpha}(V) \quad (1)$$

with

$$\Delta H_{\mathrm{mix},\alpha}(x) = \Delta H_{\mathrm{poly},\alpha}(x) + \Delta H_{\Omega,\alpha}(x) \quad (2)$$

Here, $\Delta H_{\mathrm{poly},\alpha}(x) = (1-x)\,\Delta E_{A,\alpha} + x\,\Delta E_{B,\alpha}$ is the ideal component of the mixing enthalpy, determined as the polymorph energy interpolated between the end-member compounds; $\Delta H_{\Omega,\alpha}(x) = \Omega_\alpha\, x(1-x)$ is the nonideal component of the mixing enthalpy arising from interactions between dissimilar substituents of the alloy, with the interaction parameter Ω_α quantifying the enthalpic strength of these interactions and the resulting bowing of the mixing enthalpy; and $\Delta H_{vol}(V)$ is the energetic contribution from volume changes (see the Supplementary Materials for details). Figure 1A shows the $\Delta H(V)$ projection of $\Delta H(V,x)$ for the three considered polymorphs at $x = 0$, and Fig. 1B shows the $\Delta H(x)$ projection of $\Delta H(V,x)$ for the equilibrium volume of the respective phase at each composition.

The nonideal component of mixing enthalpy $\Delta H_\Omega(x)$ depends on the crystal structure of the alloy: Lower-density structures tend to have smaller alloy interaction parameters Ω owing to less competition for space between the atoms [that is, less steric hindrance (*19*)]. In turn, the evolution of the enthalpy as a function of composition is different for each polymorph, with the lower-density structure showing a smaller bowing of the mixing enthalpy. Consequently, as shown in Fig. 1B, the metastable lower-density γ polymorph can become the most stable solid solution structure at intermediate concentrations in an alloy system $A_{1-x}B_x$. This general analysis indicates that heterostructural alloying should provide a route to negative-pressure polymorphs with lower-density structures.

At absolute zero temperature ($T = 0$ K) depicted in Fig. 1, stabilization of the γ polymorph at $A_{1-x}B_x$ composition would also require a kinetic barrier that prevents its decomposition into the α polymorph of compound A and the β polymorph of compound B. However, at more realistic synthesis temperatures, the stability of polymorphs is defined by their Gibbs free energy $\Delta G = \Delta H - T\Delta S$, where ΔH is the enthalpy discussed above and ΔS is the entropy. Therefore, in reality, the lowest-enthalpy γ polymorph at $A_{1-x}B_x$ composition would be further stabilized by the increased configurational entropy of the alloy with respect to the pure compounds A and B. The configurational (ΔS_{conf}) and vibrational (ΔS_{vibr}) entropy terms of the alloys are likely to be similar among the different polymorphs, such that the differences in free energy ΔG are dominated by the differences in enthalpies ΔH.

Figure 1C summarizes the dependence of the alloy enthalpy $\Delta H(V,x)$ on both chemical composition x and atomic volume V for the three considered polymorphs. Selecting the minimum enthalpy $\Delta H_{min}(V,x)$ among the three polymorphs for each coordinate (V,x), the basins of attraction can be drawn as shown on gray scale in Fig. 1C, highlighting how the γ polymorph becomes energetically favorable for intermediate alloying concentrations. This heterostructural alloying method to achieve negative-pressure polymorphs does not require impractically large tensile strains unlike mechanical methods and is not limited by critical film thickness and the choice of substrate unlike epitaxial methods.

Downloaded from http://advances.sciencemag.org/ on May 11, 2018

Composition and crystal structure

To demonstrate how heterostructural alloying can lead to negative-pressure polymorphs, we predicted and synthesized the Mn(Se,Te) alloy with a previously unreported low-density structure. The MnSe-MnTe materials system was chosen because according to theoretical calculations (see table S1), the wurtzite (WZ), RS, and nickeline (NC) structures for both MnSe and MnTe are energetically close (differences, <30 meV per atom). Notably, the WZ structure has an almost 30% larger atomic volume compared to that of the RS and NC structures. According to experimental literature, MnSe is most stable in the cubic low-volume RS-type structure, whereas other polymorphs could be experimentally realized by epitaxial growth (*20*) and in colloidal nanoparticles (*21*). MnTe crystallizes in the hexagonal low-volume NC-type structure (α-MnTe), whereas, at higher temperature and pressure, it forms in RS-type structures (β-MnTe) (*22*). Taking into account these MnSe and MnTe polymorph orderings from experimental literature, and the close calculated spacing of polymorph enthalpies (table S1), the design principle outlined in Fig. 1 would predict that the high-volume WZ structure may become energetically favorable for intermediate Mn(Se,Te) alloying concentrations, creating effective negative-pressure conditions. The loss of crystal inversion symmetry going from NC-type MnTe and RS-type MnSe structures to the WZ-type Mn(Se,Te) structure should enable new functionality, such as the piezoelectric response. The resulting optoelectronic properties of the WZ-Mn(Se,Te) alloys are also expected to differ from the parent RS-MnSe and NC-MnTe compounds due to the larger atomic volume and different atom coordination environments (tetrahedral in WZ versus octahedral in RS and NC).

To determine how the minimum enthalpy of Mn(Se,Te) varies with volume and composition (Fig. 1C), we performed first-principles calculations of the RS, WZ, and NC polymorph enthalpies and their Mn(Se,Te) alloy interaction parameters (see table S1 for the results). Because standard density functional theory (DFT) often finds incorrect ground states in transition metal compounds (*23*), we used calculations in the random phase approximation (RPA) (*24*), including a wave function optimization approach (see the Supplementary Materials for computational details) (*25*). Figure 2A shows on the color scale the lowest enthalpy among the three considered polymorphs as a function of the atomic volume (*y* axis) and the alloy concentration (*x* axis), calculated using the Murnaghan equation of state. We find that the evolution of the minimum enthalpy ΔH_{min} as a function of composition and volume is largely governed by the difference in bowing ΔH_{Ω} of the alloy mixing enthalpies ΔH_{mix}, rather than the small differences from the compound polymorph enthalpies ΔH_{poly} (table S1), which is consistent with Fig. 1. The WZ structure shows a much smaller bowing ΔH_{Ω}, which is caused by the lower steric interactions of the substituents in the higher-volume structure; that is, the WZ structure has smaller alloy interaction parameters Ω than RS and NC structures. For intermediate alloying concentrations, the high–atomic volume WZ-type $MnSe_{1-x}Te_x$ polymorph [Ω_{WZ} = 81 meV/f.u. (formula unit)] becomes energetically favorable compared to the two low–atomic volume structures of the parent RS-type MnSe and NC-type MnTe compounds (Ω_{RS} = 173 meV/f.u., Ω_{NC} = 166 meV/f.u.), similar to the situation conceptualized in Fig. 1B. In the case of Mn(Se,Te), an enthalpy difference ΔH of 10 meV per atom is observed for an alloying concentration of x = 0.5. This enthalpy difference creates a thermodynamic driving force toward the lower-density, high–atomic volume WZ-type polymorph, which should facilitate its synthesis.

To synthesize the predicted WZ-Mn(Se,Te) polymorph, high-throughput combinatorial thin-film experiments (*26*) were carried out. Figure 2B shows the resulting structure-composition relationship for thin films deposited at 320°C on glass substrates and cooled to room temperature at a rate of ~30°C/min. According to x-ray diffraction (XRD), the MnSe films crystallize in an RS structure, the MnTe films crystallize in an NC structure, and the respective peaks shift with increasing alloying concentration *x*. For intermediate compositions, a strong additional peak is observed at 2θ = 26°, whereas the NC and the RS peaks decrease in intensity. Extrapolating the simulated (002) peak of the calculated hypothetical MnSe (2θ = 27°) and MnTe (2θ = 25°) WZ structures according to Vegard's law and using the disappearing phase method (*27*), it can be concluded that the WZ-Mn(Se,Te) structure is present for $0.31 < x < 0.75$ compositions. High-resolution XRD measurements in a broad range of polar (or χ) angles performed at the Stanford Synchrotron Radiation Lightsource (SSRL) (Fig. 3A) show all characteristic peaks of the WZ structure and confirm that the low-density polymorphs were stabilized at the $MnSe_{0.5}Te_{0.5}$ composition.

Figure 3B shows the fraction of the WZ phase as a function of substrate temperature and alloying composition *x*, calculated by integrating the area under the WZ, NC, and RS peaks in the 2θ = 23.25° to 34.25° range. At high temperature (500°C), a binodal decomposition of WZ-type Mn(Se,Te) into RS-type MnSe and NC-type MnTe is observed (see fig. S1), with phase boundaries that are in agreement with previous results in the literature (*28*). At a lower synthesis temperature (300° to 400°C), this decomposition must be kinetically hindered, because the majority WZ phase with minority RS and NC impurity peaks is observed. Thus, it appears that at these lower synthesis temperatures and relatively slow cooling rates (~30°C/min), the WZ-Mn(Se,Te) negative-pressure polymorph is stabilized by both thermodynamic driving force

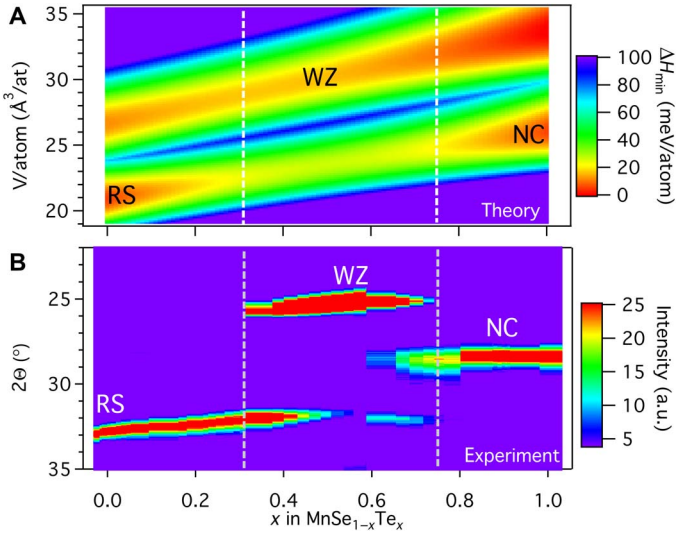

Fig. 2. Stabilization of the WZ polymorph of the Mn(Se,Te) alloy. (**A**) Calculated minimum enthalpy ΔH_{min} of $MnSe_{1-x}Te_x$ alloys on the color scale as a function of volume *V* and composition *x*. For intermediate compositions, the higher-volume WZ structure becomes energetically favorable compared to lower-volume RS and NC structures, like under negative-pressure conditions. (**B**) Measured false-color plot of XRD intensities as a function of composition for the $MnSe_{1-x}Te_x$ films deposited at 320°C. For intermediate compositions, the Mn(Se,Te) films crystallize mostly in the WZ structure, whereas the MnSe and MnTe parent compounds crystallize in RS and NC structures.

Downloaded from http://advances.sciencemag.org/ on May 11, 2018

toward its low-density structure and kinetic barriers that prevent its decomposition into constituent RS-MnSe and NC-MnTe phases, as hypothesized in Fig. 1B. To achieve thermodynamic stability of the WZ-Mn(Se,Te) negative-pressure polymorph with respect to RS-MnSe and NC-MnTe, by both enthalpic and entropic contributions to the Gibbs free energy, higher synthesis temperatures and faster quenching rates would be needed.

Properties and potential applications

Next, we show that the nonmonotonic changes in physical properties of the resulting WZ-$MnSe_{0.5}Te_{0.5}$ heterostructural alloys (Table 1) are distinct from the conventional case of isostructural alloying (for example, zincblende $ZnS_{1-x}Se_x$). The most remarkable change in the properties is the emergence of the piezoelectric response in the WZ-$MnSe_{0.5}Te_{0.5}$ alloy that is not present in either of the RS-MnSe or NC-MnTe parent compounds. Our theoretical calculations predict an effective piezoelectric coefficient d_{33} of 9.54 pm/V for the WZ-$MnSe_{0.5}Te_{0.5}$ alloys, and no piezoelectric response for the end-member compounds with NC and RS crystal structures. Qualitative piezo force microscopy (PFM) imaging on WZ-$MnSe_{0.5}Te_{0.5}$ thin films shows an abrupt change in the polarity of the film across the domain boundaries, confirming the piezoelectric response of the material (fig. S2). Quantitative PFM measurements of the WZ-$MnSe_{0.5}Te_{0.5}$ samples as a function of bias voltage calibrated by the $BiFeO_3$ reference samples place the estimated d_{33} in the range from 1.5 to 11 pm/V, consistent with the value obtained from the theoretical calculations. These values are in the same order of magnitude as the piezoelectric coefficients for *x*-cut quartz (2.2 pm/V), and *c*-axis–oriented AlN (4.9 pm/V) or ZnO (9.9 pm/V), placing WZ-$MnSe_{0.5}Te_{0.5}$ alloys among the few simple lead-free piezoelectric materials known to date. These materials are of importance for sensors and actuators in telecommunication components and for many other industrial applications.

In addition to piezoelectric response, the WZ-$MnSe_{0.5}Te_{0.5}$ alloys also have different optoelectronic properties compared to RS-type MnSe and NC-type MnTe parent compounds (Fig. 4). Theoretically, density-of-states (DOS) calculations show that the electron effective mass m_e* is reduced by 2×–4× from 0.78–1.26 m_0 to 0.30 m_0, whereas the hole effective mass m_h* for the alloy remains approximately unaltered (1.5 to 1.8 m_0). Materials with low effective masses and high mobilities are important for many electronic applications, such as transistors. In addition, the calculated optical band gap of WZ-type $MnSe_{0.5}Te_{0.5}$ alloys (2.70 eV) is wider than that for both NC-type MnTe (1.45 eV) and RS-type MnSe (2.50 eV), consistent with optical and electrical experimental measurements (fig. S3). These band gaps and effective masses make WZ-$MnSe_{0.5}Te_{0.5}$ alloys interesting as contact material for thin-film solar cells. Good semiconductor properties of the negative-pressure polymorphs also might be of interest in thermoelectric energy conversion, where low thermal conductivities of low-density structures are desirable. MnTe-SnTe alloys in RS structures have been recently demonstrated to have large thermoelectric figures of merit (*29*), which may be further enhanced in WZ-based alloys with lower thermal conductivities.

To explain the differences in electronic properties with the changes in crystal structure, we turn to the DOS calculations (Fig. 4). The sixfold coordination in RS and NC structures causes stronger hybridization between the Mn *d*-states and the Se or Te *p*-states than in the fourfold coordinated WZ structure. These stronger interactions of the Mn states with e_g symmetry create bonding and antibonding energy shoulders around the main t_{2g} peaks, thereby increasing effective masses, both

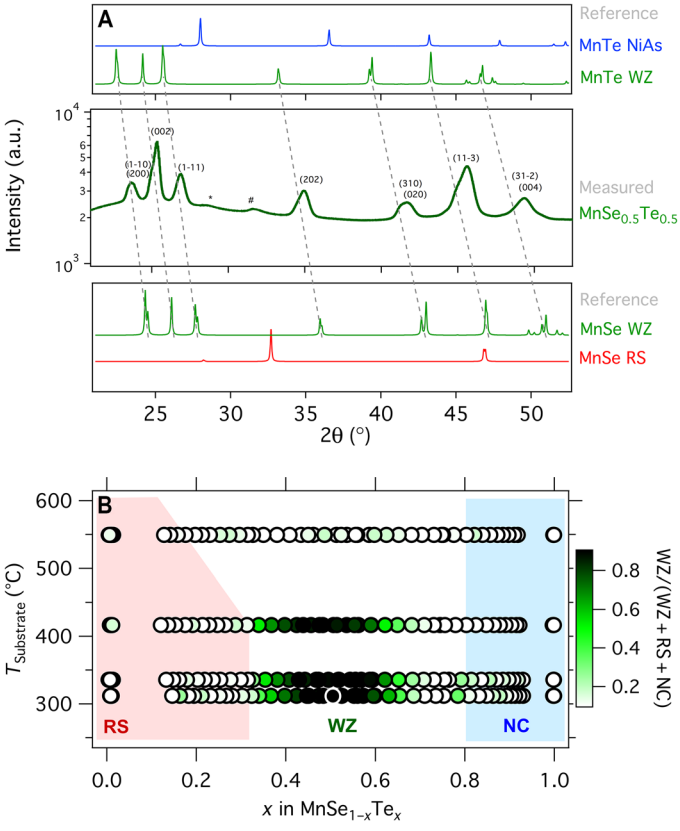

Fig. 3. Experimental crystal structure analysis of $MnSe_{1-x}Te_x$ alloys. (**A**) Synchrotron XRD measurements of $MnSe_{0.5}Te_{0.5}$ thin films grown on glass at 320°C substrate temperature [black circle with white boarder in (B)] confirm the stabilization of the high-enthalpy, low-density WZ polymorph. Trace amounts of MnTe NC (*) and MnSe RS (#) could be present in the film. The top and the bottom panels show the simulated XRD patterns of MnSe and MnTe in WZ and other structures, and the dashed lines are extrapolations of the WZ peaks. (**B**) Color-scale map of the WZ phase fraction for the sputter-deposited $MnSe_{1-x}Te_x$ thin films on glass. For intermediate compositions and lower deposition temperatures, the $MnSe_{1-x}Te_x$ films crystallize predominantly in the WZ structure with some RS- and NC-type impurities. Shaded areas represent single-phase regions of RS-MnSe and NC-MnTe determined by the disappearing phase method.

Table 1. Properties for the WZ-type $MnSe_{0.5}Te_{0.5}$ alloys compared to the RS-type MnSe and NC-type MnTe parent compounds. Listed are the calculated direct (d) or indirect (i) electronic band gaps (E_g^{el}), the hole and electron effective masses (m_e* and m_h*), the calculated and measured piezoelectric coefficient (d_{33}), and experimentally determined values for the optical band gaps (E_g^{opt}). The results of experimental measurements of piezoelectric response and electrical resistivity are provided in figs. S2 and S3.

Materials	d_{33} (pm/V)	d_{33} (pm/V)	m_e*/m_0	m_h*/m_0	E_g^{el} (eV)	E_g^{opt} (eV)
Polymorph	Theory	Experiment	Theory	Theory	Theory	Experiment
RS-MnSe	—	—	0.78	1.57	2.52 (i)	2.50
WZ-$MnSe_{0.5}Te_{0.5}$	9.54	1.5–11	0.30	1.80	2.71 (d)	2.70
NC-MnTe	—	—	1.26	1.54	0.98 (i)	1.45

Downloaded from http://advances.sciencemag.org/ on May 11, 2018

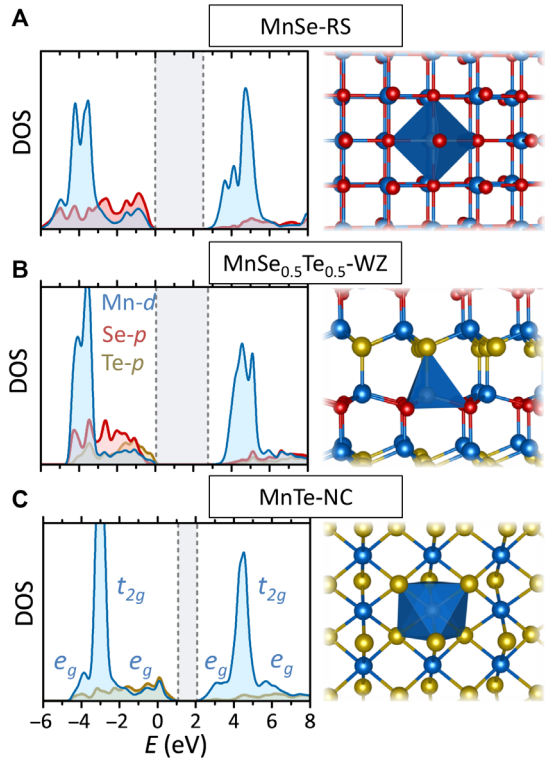

Fig. 4. Theoretical electronic and crystal structures of the Mn(Se,Te) materials. (**A**) MnSe in the RS crystal structure, (**B**) $MnSe_{0.5}Te_{0.5}$ in the WZ crystal structure, and (**C**) MnTe in the NC crystal structure. The larger band gap and smaller electron effective mass of the WZ-Mn(Se,Te) alloy result from weaker *p-d* hybridization of the Mn *d*-states of e_g symmetry with the Se,Te *p*-states. In turn, the weaker hybridization is caused by tetrahedral coordination of the lower–atomic density WZ structure compared to the octahedral coordination of the RS-MnSe and NC-MnTe structures.

in the valence band (VB) and in the conduction band, and reducing the band gaps. The increase in hole effective masses is counteracted by increased dispersion close to the VB maximum (~0.2 eV) due to strong *p-d* interaction, similar to MnO (*30*). The net result of these two competing effects is the wider band gap and the smaller electron effective mass in the tetrahedrally bonded WZ-Mn(Se,Te) alloy, compared to those in the octahedrally bonded RS-MnSe and NC parent compounds (Table 1). This coordination and symmetry analysis of the electronic structure provides a useful insight into the design of transition metal compounds with favorable semiconductor properties. Besides optoelectronic and piezoelectric applications, WZ-Mn(Se,Te) alloys may also be of interest for magnetic memory applications, where NC-MnTe has been recently studied (*31*).

DISCUSSION

We have shown how negative-pressure polymorphs can be made using heterostructural alloying. These low-density structures can be stabilized at intermediate alloy composition due to a lower bowing of the mixing enthalpy compared to high-density structures (Fig. 1), which should work equally well for both low-temperature thin films and high-temperature bulk materials. The low bowing of the mixing enthalpy results from less competition for space between the atoms in the low-density structures. As a proof of principle, we have calculated and synthesized metastable WZ-type Mn(Se,Te) polymorph with high atomic volumes (Fig. 2) by alloying RS-type MnSe and NC-type MnTe compounds with low atomic volumes in thin-film form (Fig. 3). The change in structure from RS/NC type to WZ type led to the emergence of the piezoelectric effect that does not exist in the parent compounds (Table 1) and to a combination of optical band gaps and effective masses suitable for photovoltaic contact applications (Fig. 4). In addition to optoelectronics and piezoelectrics, the new WZ-Mn(Se,Te) material may be used in magnetic memory and thermoelectric applications.

Mixing two materials with different crystal structures remains a rather unexplored area in ceramic conductor (*32*) and semiconductor (*16*) alloys, where the energy scale of polymorph energies and mixing enthalpies are usually much higher than those in metal alloys (*33*). The results of this work go well beyond the previously published studies on semiconductor heterostructural alloying (*16*–*18*) because, here, an entirely new third material [WZ-Mn(Se,Te)] has been discovered at intermediate alloy compositions, under conditions equivalent to effective negative pressure. The nonmonotonic changes of properties discussed here also make these heterostructural semiconductor alloys distinct from isostructural semiconductor alloys used to continuously tune properties for optoelectronic applications (for example, III-V alloys for light-emitting diodes and solid-state lasers).

It is likely that the heterostructural alloying approach can be extended to many other material systems, where high-enthalpy structures with desired functionalities are predicted to be stable at negative pressures, opening a virgin phase space to design new materials for electronic applications. For example, high-throughput computational databases [for example, NRELMatDB (https://materials.nrel.gov/) or Materials Project (https://materialsproject.org/)] could be screened for other II-VI and III-V material combinations, where a crossover of polymorph mixing enthalpies is predicted because of a specific polymorph ordering (Fig. 1B). As shown in this study, it is also likely that such crossovers can occur because of the large differences in the bowings of mixing enthalpies for different polymorphs, even in the absence of substantial polymorph enthalpy differences. A broad material screening study using these selection criteria would likely allow access to useful properties in numerous other negative-pressure polymorphs that are otherwise nearly impossible to make.

MATERIALS AND METHODS

Experiments

High-throughput combinatorial experiments (*26*) were used as a time-efficient way to investigate the composition-temperature synthesis phase space of the MnSe-MnTe materials system. By applying intentional mutually orthogonal gradients in deposition temperature and chemical composition across the substrates during thin-film synthesis (*34*), many values of these deposition parameters were covered in a single experiment. Several thin-film combinatorial libraries were deposited on amorphous glass substrates using radio-frequency co-sputtering from ceramic MnSe and MnTe targets to cover a broad range of deposition temperatures and alloy compositions, ruling out potential effects from lattice mismatch and thermal stress on WZ phase stabilization. Each library was analyzed at 44 sample positions via spatially resolved x-ray fluorescence and XRD for their chemical composition and crystal structure. The optoelectronic properties were mapped using ultraviolet-visible optical transmission, four-point probe sheet resistance, and Seebeck measurements (*35*). A more detailed description of these combinatorial experimental methods, as well as single-point synchrotron XRD and PFM analysis, can be found in the Supplementary Materials.

Downloaded from http://advances.sciencemag.org/ on May 11, 2018

Computations

To computationally model the alloys, the special quasi-random structure (SQS) method (*36*) was used to generate ideally random alloy structures for each phase and composition. The alloy mixing enthalpy, bowings, and interaction parameter calculations were performed using 128-atom SQS models. These energies, as well as piezoelectric and elastic properties, were calculated in DFT + U with $U = 3$ eV for Mn-d orbitals, using the VASP (Vienna Ab initio Simulation Package) code (*37*). Calculations of the elastic tensors (C_{kj}) were performed using the stress-strain method (*38*), and the piezoelectric responses (e_{ij}) were computed within the density-functional perturbation theory formalism (*39*); the reported piezoelectric tensor component (d_{33}) was determined from the tensor relation $e_{ij} = \sum_k d_{ik} C_{kj}$. The polymorph enthalpies of the parent compounds were computed using the RPA (*24*) with a variational optimization of the wave function that correctly recovers the Mn-d/anion-p hybridization (*25*) of each MnSe and MnTe polymorph, taking into account zero-point energy corrections. The Green's Function (GW) based calculations were performed as described by Peng and Lany (*30*). Additional details of the computational methods used in this work are available in the Supplementary Materials.

SUPPLEMENTARY MATERIALS

Supplementary material for this article is available at http://advances.sciencemag.org/cgi/content/full/4/4/eaaq1442/DC1

Supplementary Methods

Supplementary Additional Results

table S1. Polymorph energies from DFT and RPA calculations and the magnitude of zero-point energies from the QHA.

fig. S1. Detailed XRD study performed on $MnSe_{0.5}Te_{0.5}$ grown on indium tin oxide (ITO)–coated Eagle XG glass.

fig. S2. PFM measurements of a WZ-$MnSe_{0.5}Te_{0.5}$ film grown on conductive ITO substrate.

fig. S3. Optoelectronical characterization of Mn(Se,Te) alloys.

REFERENCES AND NOTES

1. K. Vonnegut, *Cat's Cradle* (Holt, Rinehart & Winston, 1963).
2. A. E. Goresy, M. Chen, L. Dubrovinsky, P. Gillet, G. Graup, An ultradense polymorph of rutile with seven-coordinated titanium from the Ries crater. *Science* **293**, 1467–1470 (2001).
3. M. A. Neumann, J. van de Streek, F. P. A. Fabbiani, P. Hidber, O. Grassmann, Combined crystal structure prediction and high-pressure crystallization in rational pharmaceutical polymorph screening. *Nat. Commun.* **6**, 7793 (2015).
4. S. H. Friedman,. The four worlds of carbon. *Nat. Chem.* **4**, 426–426 (2012).
5. A. Fujishima, K. Honda, Electrochemical photolysis of water at a semiconductor electrode. *Nature* **238**, 37–38 (1972).
6. W. Sun, S. T. Dacek, S. P. Ong, G. Hautier, A. Jain, W. D. Richards, A. C. Gamst, K. A. Persson, G. Ceder, The thermodynamic scale of inorganic crystalline metastability. *Sci. Adv.* **2**, e1600225 (2016).
7. Y. Ma, M. I. Eremets, A. R. Oganov, Y. Xie, I. Trojan, S. Medvedev, A. O. Lyakhov, M. Valle, V. Prakapenka, Transparent dense sodium. *Nature* **458**, 182–185 (2009).
8. C. H. Bates, W. B. White, R. Roy, New high-pressure polymorph of zinc oxide. *Science* **137**, 993 (1962).
9. D. G. Schlom, C. J. Fennie, Ferroelectrics: The positives of going negative. *Nat. Mater.* **14**, 969–970 (2015).
10. O. Y. Gorbenko, S. V. Samoilenkov, I. E. Graboy, A. R. Kaul, Epitaxial stabilization of oxides in thin films. *Chem. Mater.* **14**, 4026–4043 (2002).
11. J. E. Ayers, *Heteroepitaxy of Semiconductors: Theory, Growth, and Characterization* (CRC Press, 2007).
12. A. Falenty, T. C. Hansen, W. F. Kuhs, Formation and properties of ice XVI obtained by emptying a type sII clathrate hydrate. *Nature* **516**, 231–233 (2014).
13. A. M. Guloy, R. Ramlau, Z. Tang, W. Schnelle, M. Baitinger, Y. Grin, A guest-free germanium clathrate. *Nature* **443**, 320–323 (2006).
14. S. A. Kimber, A. Kreyssig, Y. Z. Zhang, H. O. Jeschke, R. Valentí, F. Yokaichiya, E. Colombier, J. Yan, T. C. Hansen, T. Chatterji, R. J. McQueeney, P. C. Canfield, A. I. Goldman, D. N. Argyriou, Similarities between structural distortions under pressure and chemical doping in superconducting $BaFe_2As_2$. *Nat. Mater.* **8**, 471–475 (2009).
15. J. Wang, B. Wylie-van Eerd, T. Sluka, C. Sandu, M. Cantoni, X.-K. Wei, A. Kvasov, L. J. McGilly, P. Gemeiner, B. Dkhil, A. Tagantsev, J. Trodahl, N. Setter, Negative-pressure-induced enhancement in a freestanding ferroelectric. *Nat. Mater.* **14**, 985–990 (2015).
16. H. Peng, P. F. Ndione, D. S. Ginley, A. Zakutayev, S. Lany, Design of semiconducting tetrahedral $Mn_{1-x}Zn_xO$ alloys and their application to solar water splitting. *Phys. Rev. X* **5**, 021016 (2015).
17. A. M. Holder, S. Siol, P. F. Ndione, H. Peng, A. M. Deml, B. E. Matthews, L. T. Schelhas, M. F. Toney, R. G. Gordon, W. Tumas, J. D. Perkins, D. S. Ginley, B. P. Gorman, J. Tate, A. Zakutayev, S. Lany, Novel phase diagram behavior and materials design in heterostructural semiconductor alloys. *Sci. Adv.* **3**, e1700270 (2017).
18. B. E. Matthews, A. M. Holder, L. T. Schelhas, S. Siol, J. W. May, M. R. Forkner, D. Vigil-Fowler, M. F. Toney, J. D. Perkins, B. P. Gorman, A. Zakutayev, S. Lany, J. Tate, Using heterostructural alloying to tune the structure and properties of the thermoelectric $Sn_{1-x}Ca_xSe$. *J. Mater. Chem. A* **5**, 16873–16882 (2017).
19. S. Lany, Polymorphism, band-structure, band-lineup, and alloy energetics of the group II oxides and sulfides MgO, ZnO, CdO, MgS, ZnS, CdS. *Proc. SPIE* **8987**, 89870K (2014).
20. D. Litvinov, D. Gerthsen, A. Rosenauer, B. Daniel, M. Hetterich, Sphalerite-rock salt phase transition in ZnMnSe heterostructures. *Appl. Phys. Lett.* **85**, 751–753 (2004).
21. I. T. Sines, R. Misra, P. Schiffer, R. E. Schaak, Colloidal synthesis of non-equilibrium wurtzite-type MnSe. *Angew. Chem. Int. Ed. Engl.* **49**, 4638–4640 (2010).
22. M. Krause, F. Bechstedt, Structural and magnetic properties of MnTe phases from ab initio calculations. *J. Supercond. Nov. Magn.* **26**, 1963–1972 (2013).
23. A. Schrön, C. Rödl, F. Bechstedt, Energetic stability and magnetic properties of MnO in the rocksalt, wurtzite, and zinc-blende structures: Influence of exchange and correlation. *Phys. Rev. B* **82**, 165109 (2010).
24. J. Harl, G. Kresse, Accurate bulk properties from approximate many-body techniques. *Phys. Rev. Lett.* **103**, 056401 (2009).
25. H. Peng, S. Lany, Polymorphic energy ordering of MgO, ZnO, GaN, and MnO within the random phase approximation. *Phys. Rev. B* **87**, 174113 (2013).
26. M. L. Green, I. Takeuchi, J. R. Hattrick-Simpers, Applications of high throughput (combinatorial) methodologies to electronic, magnetic, optical, and energy-related materials. *J. Appl. Phys.* **113**, 231101 (2013).
27. B. D. Cullity, *Elements of X-ray Diffraction* (Addison-Wesley Publishing Company, ed. 2, 1978).
28. A. J. Panson, W. D. Johnston, The MnTe MnSe system. *J. Inorg. Nucl. Chem.* **26**, 701–703 (1964).
29. G. Tan, F. Shi, S. Hao, H. Chi, T. P. Bailey, L. D. Zhao, C. Uher, C. Wolverton, V. P. Dravid, M. G. Kanatzidis, Valence band modification and high thermoelectric performance in SnTe heavily alloyed with MnTe. *J. Am. Chem. Soc.* **137**, 11507–11516 (2015).
30. H. Peng, S. Lany, Semiconducting transition-metal oxides based on d^5 cations: Theory for MnO and Fe_2O_3. *Phys. Rev. B* **85**, 201202 (2012).
31. D. Kriegner, K. Výborný, K. Olejník, H. Reichlová, V. Novák, X. Marti, J. Gazquez, V. Saidl, P. Němec, V. V. Volobuev, G. Springholz, V. Holý, T. Jungwirth, Multiple-stable anisotropic magnetoresistance memory in antiferromagnetic MnTe. *Nat. Commun.* **7**, 11623 (2016).
32. C. M. Rost, E. Sachet, T. Borman, A. Moballegh, E. C. Dickey, D. Hou, J. L. Jones, S. Curtarolo, J. P. Maria, Entropy-stabilized oxides. *Nat. Commun.* **6**, 8485 (2015).
33. Z. Li, K. G. Pradeep, Y. Deng, D. Raabe, C. C. Tasan, Metastable high-entropy dual-phase alloys overcome the strength–ductility trade-off. *Nature* **534**, 227–230 (2016).
34. A. Subramaniyan, J. D. Perkins, R. P. O'Hayre, S. Lany, V. Stevanovic, D. S. Ginley, A. Zakutayev, Non-equilibrium deposition of phase pure Cu_2O thin films at reduced growth temperature. *APL Mater.* **2**, 022105 (2014).
35. A. Zakutayev, F. J. Luciano IV, V. P. Bollinger, A. K. Sigdel, P. F. Ndione, J. D. Perkins, J. J. Berry, P. A. Parilla, D. S. Ginley, Development and application of an instrument for spatially resolved Seebeck coefficient measurements. *Rev. Sci. Instrum.* **84**, 053905 (2013).
36. A. Zunger, S. Wei, L. G. Ferreira, J. E. Bernard, Special quasirandom structures. *Phys. Rev. Lett.* **65**, 353–356 (1990).
37. J. P. Perdew, K. Burke, M. Ernzerhof Generalized gradient approximation made simple. *Phys. Rev. Lett.* **77**, 3865–3868 (1996).
38. Y. Le Page, P. Saxe, Symmetry-general least-squares extraction of elastic data for strained materials from ab initio calculations of stress. *Phys. Rev. B* **65**, 104104 (2002).
39. X. Wu, D. Vanderbilt, D. R. Hamann Systematic treatment of displacements, strains, and electric fields in density-functional perturbation theory. *Phys. Rev. B* **72**, 035105 (2005).

Acknowledgments: We thank J. Tate, V. Stevanovic, E. Toberer, and D. Ginley for helpful discussions. **Funding:** This work was supported by the U.S. Department of Energy, Office of Science, Office of Basic Energy Sciences, as part of the Energy Frontier Research Center "Center for Next Generation of Materials by Design" under contract no. DE-AC36-08GO28308 to the National Renewable Energy Laboratory (NREL). P.A.P. acknowledges support from NREL's Laboratory Directed Research and Development (LDRD) program under grant no. 06591403. J.S. and B.D.H.

Downloaded from http://advances.sciencemag.org/ on May 11, 2018

were supported by the GE-UConn Fellowship for Innovation Consortium. Use of the SSRL, SLAC National Accelerator Laboratory, was supported by the U.S. Department of Energy, Office of Science, Office of Basic Energy Sciences under contract no. DE-AC02-76SF00515. High-performance computing resources were sponsored by the U.S. Department of Energy, Office of Energy Efficiency and Renewable Energy. **Author contributions:** S.S. and A.Z. led the project and wrote the manuscript with input from W.T. and all the other co-authors. S.S., A.H., A.Z., and S.L. conceptualized the approach of creating negative-pressure polymorph through heterostructural alloying. A.H. and S.L. performed the computational work. S.S. performed the combinatorial thin-film synthesis, characterization, and analysis with contributions from A.Z. J.D.P. and P.A.P. assisted with the laboratory XRD measurements. L.T.S., K.H.S., and M.F.T. performed the synchrotron XRD experiments. J.S. and B.D.H. performed the PFM measurements and analysis with contributions from L.G. **Competing interests:** The authors declare that they have no competing interests. **Data and materials availability:** All data needed to evaluate the conclusions in the paper are present in the paper and/or the Supplementary Materials. Additional data related to this paper is available at https://materials.nrel.gov and https://htem.nrel.gov or may be requested from the authors.

Submitted 6 October 2017
Accepted 7 March 2018
Published 20 April 2018
10.1126/sciadv.aaq1442

Citation: S. Siol, A. Holder, J. Steffes, L. T. Schelhas, K. H. Stone, L. Garten, J. D. Perkins, P. A. Parilla, M. F. Toney, B. D. Huey, W. Tumas, S. Lany, A. Zakutayev, Negative-pressure polymorphs made by heterostructural alloying. *Sci. Adv.* **4**, eaaq1442 (2018).

Downloaded from http://advances.sciencemag.org/ on May 11, 2018

ScienceAdvances

Negative-pressure polymorphs made by heterostructural alloying

Sebastian Siol, Aaron Holder, James Steffes, Laura T. Schelhas, Kevin H. Stone, Lauren Garten, John D. Perkins, Philip A. Parilla, Michael F. Toney, Bryan D. Huey, William Tumas, Stephan Lany and Andriy Zakutayev

Sci Adv **4** (4), eaaq1442.
DOI: 10.1126/sciadv.aaq1442

ARTICLE TOOLS http://advances.sciencemag.org/content/4/4/eaaq1442

SUPPLEMENTARY MATERIALS http://advances.sciencemag.org/content/suppl/2018/04/16/4.4.eaaq1442.DC1

REFERENCES This article cites 36 articles, 4 of which you can access for free
http://advances.sciencemag.org/content/4/4/eaaq1442#BIBL

PERMISSIONS http://www.sciencemag.org/help/reprints-and-permissions

Use of this article is subject to the Terms of Service

Science Advances (ISSN 2375-2548) is published by the American Association for the Advancement of Science, 1200 New York Avenue NW, Washington, DC 20005. 2017 © The Authors, some rights reserved; exclusive licensee American Association for the Advancement of Science. No claim to original U.S. Government Works. The title *Science Advances* is a registered trademark of AAAS.

Downloaded from http://advances.sciencemag.org/ on May 11, 2018